Distributions for wave overtopping parameters for stress strength analyses on flood embankments

van Damme, Myron

DOI
10.1016/j.coastaleng.2016.06.010

Publication date
2016

Document Version
Accepted author manuscript

Published in
Coastal Engineering

Citation (APA)
van Damme, M. (2016). Distributions for wave overtopping parameters for stress strength analyses on flood embankments. *Coastal Engineering*, *116*(October), 195-206. https://doi.org/10.1016/j.coastaleng.2016.06.010

Distributions for wave overtopping parameters for stress strength analyses on flood embankments

Myron van Damme

Delft University of Technology, Department of Hydraulic Engineering, Stevinweg 1, 2600 GA Delft, The Netherlands

Abstract

A process based assessment of the probability of failure of a flood embankment, as well as an assessment of the consequences of failure of an embankment require insights into the stresses on the landside slope of an embankment. These assessments are hindered by the empirical nature of the wave overtopping parameters. Failure initiation is often linked to an allowable mean overtopping discharge which forms the input for the overtopping volumes distribution. The high level of uncertainty associated with predicting the mean overtopping discharge therefore leads to high levels of uncertainty in predicting wave overtopping volumes. The mean overtopping discharge is thereby not directly related to run-up parameters. This paper addresses these issues by presenting new distributions for the velocity, discharge, depth, volume, and shear stresses at the crest for those waves that overtop which have been derived from the wave run-up parameters. The proposed distributions are independent on the mean wave overtopping discharge and the large inaccuracies associated with predicting this. The proposed method has the added benefit of being able to express overtopping parameters in terms of each other. The paper also provides a method for determining the change in these random overtopping values along the landside slope, thereby facilitatating a direct comparison between wave overtopping events and overflow events.

Keywords: Wave overtopping, distribution, volumes, discharge, shear stresses, run-up, embankment

1. Introduction

Decisions on investments in flood protection are based on flood risk analysis (Hall et al., 2003; Environment Agency, 2009; Gouldby et al., 2010; Kuijken,

2015). The risk of an embankment failing is determined by the probability of the embankment failing multiplied by the consequences of this failure. The probability of failure usually follows from a stress strength analysis. Failure is thereby defined as the moment whereby the embankment is no longer able to fulfill its design function. The consequences of failure are amongst others a function of the rate at which an embankment breaches. Embankment breach models have been developed to assess damage formation, and hence the residual strength of embankments as a function of loading due to overflow (Macchione, 2008; Wu, 2013; Singh et al., 1988; Zhu, 2006), but few methods have yet been developed to assess the damage formation of embankments due to wave overtopping (D'Eliso, 2007).

An accurate assessment of the probability of failure due to overflow or wave-overtopping, starts with a detailed assessment of the stresses exerted on the embankment in relation to the strength of the embankment. The probability of failure of an embankment under overflow has been studied in detail. For example, for a grass covered embankment, the initiation of failure has been given by relating the stresses on the grass cover to the change in strength of a grass cover with time (Dean et al., 2010; Hughes, 2011). However in the case of wave overtopping a more empirical approach is used whereby a maximum allowable mean overtopping discharge is given which has been determined experimentally. The scale parameter of the Weibull distribution used for describing the overtopping volumes is thereby a function of the mean overtopping discharge.

On the other side of the spectrum research has been performed to the wave run-up heights, velocity, depth and discharge. Van Gent (2002) attempted to relate the wave overtopping volume to wave run-up parameters but did not compare the results with the overtopping volumes that follow from the Weibull distributions. This paper relates the overtopping volume to wave run-up parameters like the run-up depth, height, and velocity. The outcome could be used to relate the overtopping volumes to stress parameters, making a process based stress strength analysis analysis possible.

The analysis presented in this paper works from the assumption that the wave overtopping volume and mean overtopping discharge are directly related to wave run-up parameters like the run-up depth, height, and velocity. It thereby assumes that the incoming waves are Rayleigh distributed. Where possible the newly derived distributions have been validated against data, among which the CLASH database (Steendam et al., 2004) which consists of a collection of outcomes of wave overtopping experiments. Probability distributions for the peak velocity, depth, discharge, overtopping volume and shear stress are derived in Section 3. The means by which each of these parameters has been determined are discussed

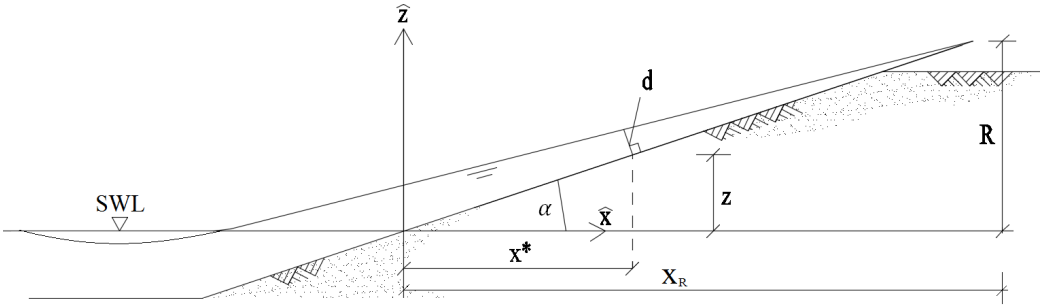

Figure 1: Definitions used in describing wave run-up (for explanations parameters see text)

in Section 2 whereby in Section 2.6 methods are discussed for converting the peak shear stress at the crest to peak shear stresses at any point along the landside slope.

2. Wave Run-up parameters

The run-up discharge [m^3/s/m], velocities [m/s], depths [m], and hence volume [m^3/m], and shear stresses [N/m^2] are related to the wave run-up height (Schüttrumpf and Oumeraci, 2005). The run-up height is here defined as the vertical distance above the still water line over which a wave travels up the assumed infinitely long waterside slope. Hunt (1959) related the run-up height of an overtopping regular wave to the wave height according to

$$R = \frac{\tan\alpha H}{\sqrt{\frac{2\pi H}{gT^2}}} \tag{1}$$

where R is the wave run-up height measured in the $\hat{z}$ direction and α is the waterside slope angle of the embankment (see Figure 1). Furthermore H [m] is the deterministic wave height of a regular wave, g [m/s^2] the gravitational constant, and T [s] the deterministic wave period. The wave run-up height, velocity, and discharge are given for a specific location (x^*, z) on the waterside slope, where x^* and z are respectively the distance in the horizontal $\hat{x}$ direction, and the vertical $\hat{z}$ direction relative to the interface of the Still Water Level (SWL). As a wave runs up the waterside slope it may reach the point (x_R, R), measured relative to the intersection of the waterside slope with the still water level. Battjes (1974) showed that for deep foreshores, the wave run-up height for relatively smooth slopes is

Rayleigh distributed. Battjes (1974) adapted the Hunt run-up formula to irregular waves, to arrive at a new methodology to be used in the Netherlands for calculating the 2% wave run-up heights for plunging breakers. This equation was later incorporated in the current standard in respectively the Netherlands and Europe, the TAW2002 (Van der Meer, 2002) and the EurOtop manual (EurOtop, 2007), as

$$\frac{R_{2\%}}{H_s} = \min\left\{1.65\gamma_b\gamma_f\gamma_\beta\xi_{m-1,0}, \gamma_f\gamma_\beta\left(4.0 - \frac{1.5}{\sqrt{\xi_{m-1,0}}}\right)\right\} \tag{2}$$

Here $R_{2\%}$ refers to the run-up height exceeded by 2% of Rayleigh distributed incoming waves, H_s [m] is the significant wave height, $\xi_{m-1,0}$ is the breaker parameter $\frac{\tan\alpha}{\sqrt{H_s/L_0}}$ where α is the waterside slope angle, and L_0 [m] is the deep water wave length given by $\frac{gT_{m-1,0}^2}{2\pi}$. Here $T_{m-1,0}$ [s] refers to the spectral period. Furthermore γ_b is a factor to account for the effects of a berm, γ_f is a factor to account for the roughness on the slope, and γ_β is a factor to account for the angle of incipient wave attack.

Relationships have been developed for the wave run-up velocities, depths, discharges, and volumes based on the run-up height R exceeded by $n\%$ of the waves, whereby n is often set at 2. The 2% run-up level alone however does not necessarily provide sufficient information on whether the scale parameter of the Rayleigh distribution is a function of normalized parameters, or a constant. Hence for the purpose of the analysis outlined in this paper the Rayleigh distribution has been fitted against wave run-up data for several exceedance probabilities to determine how the scale parameter changes for different exceedance probabilities (see Figure 2). The data was made available by Van Steeg (2015). The normalized run-up height was found to approximate a Rayleigh distribution with scale parameter 0.658, which results in the generic expression for the wave run-up height given by

$$\frac{R_{n\%}}{\epsilon H_s} = 0.93\left(-\ln\left(P\right)\right)^{\frac{1}{2}} \tag{3}$$

for

$$\epsilon = \min\left\{\xi_{m-1,0}\gamma_b\gamma_\beta\gamma_f, \frac{\gamma_f\gamma_\beta}{1.65}\left(4.0 - \frac{1.5}{\sqrt{\xi_{m-1,0}}}\right)\right\} \tag{4}$$

Here subscript n refers to the percentage of waves exceeding the run-up height R [m], and P refers to the probability that run-up exceeds the level represented by $R_{n\%}$ [m]. Based on the Rayleigh distribution for the normalized wave run-up

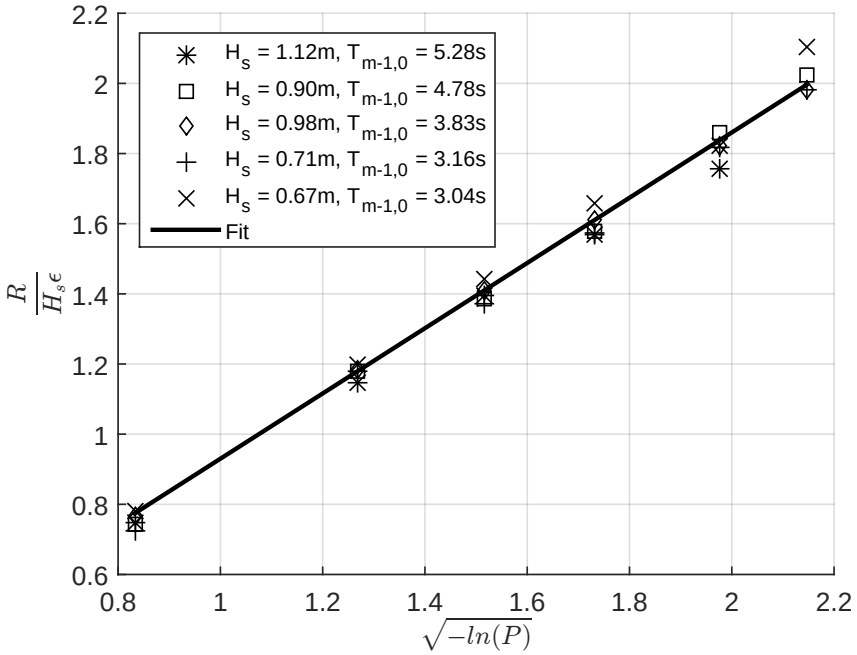

Figure 2: Fit of data against a cumulative Rayleigh run-up probability distribution (for parameters, see text))

height, relationships have been developed for the normalized wave run-up velocity, run-up depth, run-up and overtopping discharge, and run-up volume. A relationship for the run-up shear stress has also been developed using the run-up velocity and run-up depth. In the following sections each of these parameters will be discussed starting with the normalized wave run-up velocity.

2.1. Wave run-up velocity

The wave run-up velocity is defined as the peak velocity on the waterside slope measured at an arbitrary height z above the still water level during a single run-up event. The run-up velocity denoted by $u_{n\%}$ [m/s] refers to the peak run-up velocity exceeded by $n\%$ of the incoming waves. As a wave runs up a slope, kinetic energy is transferred into potential energy and dissipated due to friction and turbulence. The run-up height is therefore related to the wave run-up velocity of the front of the wave. This is moreover the peak velocity of the wave during a run-up event (Schüttrumpf and Oumeraci, 2005). The wave run-up velocity $u_{n\%}$ exceeded by $n\%$ of the incoming waves as a function of the $n\%$ run-up height is given by

$$\frac{u_{n\%}}{c_{u,n\%}\sqrt{gH_s}} = \sqrt{\frac{R_{n\%} - z}{H_s}}. \tag{5}$$

Here z is an arbitrary height on the slope below the $n\%$ run-up height $R_{n\%}$ (see Figure 1). The left hand side denotes the normalized run-up velocity exceeded by $n\%$ of the incoming waves at height z relative to the still water level. Equation 5 is based on the energy balance equation whereby the loss in energy is indicated by the $c_{u,n\%}$ parameter. An energy balance analysis has been performed to determine how $c_{u,n\%}$ changes with the run-up exceedance percentage n.

500 million normalized run-up values have been sampled from a Rayleigh distribution with scale parameter 0.658, which equals to $\sqrt{0.93^2/2}$ (see Equations 3 and 4). From the samples the conditional expected values for the run-up were calculated for those waves that exceed the $R_{n\%}$ level. Hence for the 2% run-up level this coincides with the mean potential energy of the waves that exceed the 2% run-up level $(R_{2\%})$. The results are indicated by the line 'Samples' in Figure 3. An analytical fit for this conditional distribution is given by

$$\frac{E}{\epsilon H_s} = \left[-0.88\ln\left(\frac{n}{100}\right) + 0.62\right]^{\frac{1}{2}} \tag{6}$$

where ϵ follows from Equation 4, and E [m] refers to the expected value for the potential energy of those waves that exceed the $n\%$ run-up height. The values for

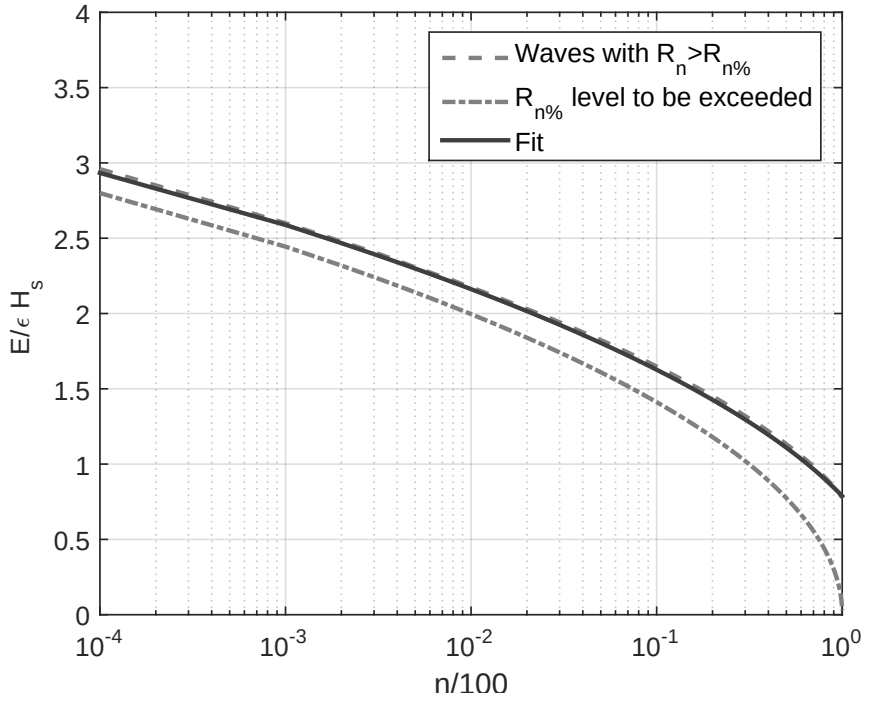

Figure 3: Expected values for the potential energy $\frac{E}{\epsilon H_s}$ for those waves that exceed the level $R_{n\%}$ (for parameter description, see text)

E that follow from Equation 6 have been normalized by dividing by the left hand side of Equations 3 for $n = 2$. This gives an expression for $\frac{E}{R_{2\%}}$. The square root of this expression multiplied by $\sqrt{2}$ gives $\sqrt{2\frac{E}{R_{2\%}}}$ which corresponds with empirical based relationships for $c_{u,2\%}$ given in the EurOtop manual. A graphical representation of this expression is denoted by the label 'Fit' in Figure 4 in which also the empirical values for $c_{u,2\%}$ from the EurOtop manual are given. The fit in

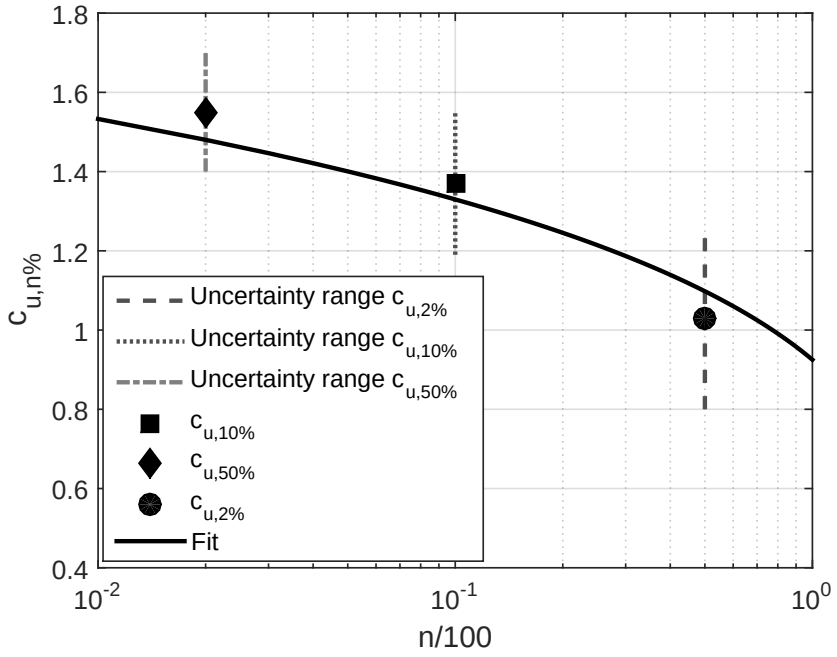

Figure 4: Empirical values versus an energy based relationship for $c_{u,n\%}$ (for parameter description see text)

Figure 4 is given by

$$c_{u,n\%} = \sqrt{\frac{2}{R_{2\%}}\left[-0.88\ln(\frac{n}{100}) + 0.62\right]^{\frac{1}{2}}} \tag{7}$$

As can be seen from Figure 4 the fit given by Equation 7 lies well within the bounds of uncertainty identified by the EurOtop manual. The values for $c_{u,10\%}$ and $c_{u,50\%}$ slightly exceed the values according to the fit whereas the value for $c_{u,2\%}$

is slightly lower. The line indicated by 'Fit' resembles the frictionless situation whereby no energy is lost. Hence any value below this line indicates a lack of kinetic energy available for reaching the required run-up height. Based on this analysis it is possible to state that the effects of friction on the run-up velocity are minor and that the run-up velocity for each individual wave is well described by a direct transformation of kinetic energy into potential energy.

Equation 5 describes the peak flow velocity at the front of the wave. When z is replaced by the crest height the peak velocity at the crest can be determined. As the wave passes over the crest the flow velocity decreases. Hughes (2011) proposed to describe the local deceleration of a wave with

$$v(t) = v_N \left(1 - \frac{t}{T_O}\right)^a \tag{8}$$

where v_N [m/s] denotes the peak velocity during an individual wave overtopping event. where T_O [s] is the total overtopping time per wave, t [s] is a time on the interval $[0, T_O]$, and a is a calibration parameter. Means of determining T_O and a are discussed later in this paper. The next parameter that will be discussed is the wave run-up depth.

2.2. Wave run-up depths

The wave run-up depth is defined as the peak depth measured during a single overtopping event at location (x^*, z) relative to the intersection between the still water level and waterside slope. The run-up depth denoted by $d_{n\%}$ [m] refers to the peak run-up depth at height z exceeded by $n\%$ of the incoming waves. Schüttrumpf and Oumeraci (2005) approximated the run-up depth $d_{n\%}$ as a linear function of the horizontal component of the wave run-up x_R [m] exceeded by $n\%$ of the incoming waves, and the horizontal component of the position x^* [m] on the waterside slope (Schüttrumpf and Oumeraci, 2005) (see Figure 1). For a straight waterside slope, the run-up depth exceeded by $n\%$ of the incoming waves can be described in terms of run-up height as (EurOtop, 2007)

$$\frac{d_{n\%}}{H_s} \frac{\tan\alpha}{c_{d,n\%}} = \frac{R_{n\%} - z}{H_s} \tag{9}$$

The left hand side here denotes the normalized run-up depth exceeded by $n\%$ of the incoming waves at height z [m]. To verify whether the run-up depth can be described by a linear function, an analysis was performed on data from a Delta flume experiment whereby run-up measurements were obtained at a rate of 50Hz

Parameter	Value
H_{m0}	0.95m
T_p	7.31s
$T_{m-1,0}$	6.37s
T_m	5.07s
s_{op}	0.011
$\xi_{m-1,0}$	3.1

Table 1: Parameters wave experiment (for parameter description see text)(Hofland et al., 2015)

using a laser scanner (Hofland et al., 2015). The flume had a length of 240m, a width of 5m, and a depth of 7m. The slope consisted of a smooth impermeable concrete layer up to 2.0m above the flume bottom, a block revetment up to 5.5m above flume bottom, and a permeable placed block revetment up to 8.3m above the flume bottom. In total 739 waves were generated from a Pierson Moskowitz spectrum for a total duration of 3770s. The vertical range covered by the laser was 2.8m. The analysed data corresponds with the test for which the parameters are given in Table 1. Here H_{m0} refers to the spectral wave height, T_p refers to the peak period, T_m to the mean wave period, and s_{op} to the wave steepness corresponding to the peak period. Using the laser scanner those moments in time were identified for which the wave run-up was maximum. At those times the gradient in water surface slope was determined per wave by dividing the difference in run-up depth between two measurement locations by the horizontal distance between the two measurement locations. As shown in Figure 5, the run-up depth gradient fluctuated around the value of 0.0751 with a standard deviation of 0.032. The difference with the gradient of 0.055 given by the EurOtop manual (EurOtop, 2007) could be attributed to the increased roughness of the block revetment. It can also be seen that near the wave front the slope decreases. Due to significant amounts of noise in the measurements those depth values below the 0.03m were eliminated from the depth database. Nonetheless these values have been used to determine the maximum run-up level (Hofland et al., 2015). The mean depth gradient near the top of the wave, between the measured maximum run-up level and the level where the depth 0.03m, was found to be 0.013 with a standard deviation of 0.0065. Despite the level of noise this shows that the run-up depth did not vary linearly with the height but appeared to be slightly concave for this case. Although the water level gradient could be obtained quite accurately using the approach, no information could be obtained with regards to a minimum value for the depth at maximum run-up due to the noise. The strong reduction in slope near

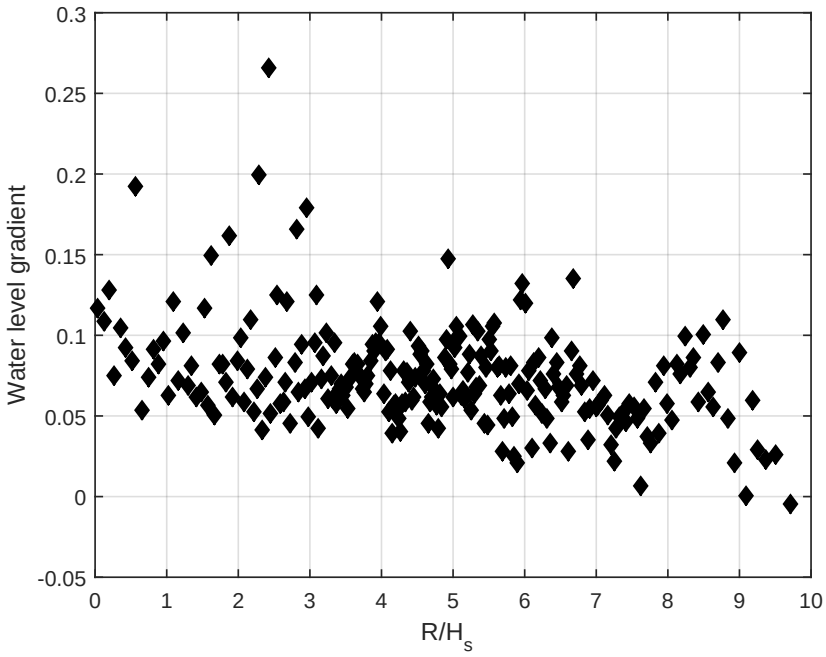

Figure 5: Datapoints for the mean gradient in run-up depth $\frac{dd}{dx}$ plotted against the normalized run-up height

the wave front may indicate a minimum depth. and a more box shaped front of the wave instead of a triangular shape. As this data confirmed that the depth gradients at maximum run-up are relatively constant, for further analysis in this paper the linear approximation from the EurOtop manual was deemed satisfactory whereby

$$\frac{d_n(x_*)}{H_s}\frac{\tan\alpha}{c_d} = \frac{R_n - z}{H_s} \tag{10}$$

where R_n [m] is the wave run-up height of the nth up-running wave, and $c_d \approx 0.055$, as follows from the relation between the $d_{2\%}$ with the $R_{2\%}$.

Similarly to the velocity distribution the overtopping depth at the intersection of the crest and waterside slope is found by replacing z by the waterside slope. Hughes et al. (2012) discovered that the overtopping depth decreases over time per wave cycle as given by

$$d(t) = d_N\left(1 - \frac{t}{T_O}\right)^b \tag{11}$$

where d_N [m] denotes the peak depth during an individual wave overtopping event. Hughes et al. (2012) found that for $b = 1$ a reasonable approximation could be obtained. In the next section the run-up velocity and run-up depth relationships are combined in discussing the wave run-up discharge and overtopping volume.

2.3. Wave run-up discharge and mean overtopping discharge

The wave run-up discharge is defined as the peak discharge measured during the passing of an up-running wave. Schüttrumpf and Oumeraci (2005) found the maximum wave run-up depth to approximately coincide with the maximum wave run-up velocity giving a maximum wave run-up discharge near the wave front. This is also the basis of the wave overtopping simulator, which releases a large amount of water from a basin under gravity (Van der Meer et al., 2006, 2008). The sudden release of water from the basin results in a wave for which the velocity and water depth are initially maximum and then decrease. Hence it is to be expected that a factor for the unit wave run-up discharge approximates the product of the factor for the wave run-up velocity $c_{u,n\%}$, and wave run-up depth $c_{d,n\%}$. The $n\%$ unit wave run-up discharge is given by

$$\frac{q_{n\%}\tan\alpha}{c_{q,n\%}\sqrt{gH_s^3}} = \left(\frac{R_{n\%} - z}{H_s}\right)^{1.5} \tag{12}$$

Here, the left hand side denotes the normalized run-up discharge. For $n = 2$, Van Gent (2002) found $c_{q,2\%} = 0.2$ which is a close approximation of the product of $c_{d,2\%}$ and $c_{u,2\%}$. This indicates that there is indeed a strong correlation between the overtopping velocity and overtopping depth. For the remainder of this paper it has been assumed that $c_{q,n\%} = c_{d,n\%} \times c_{u,n\%}$. Substituting the crest height for z gives the peak overtopping discharge. The overtopping discharge given by Equation 12 is the peak overtopping discharge. The discharge reduces with time as the wave passes. Similar to Equations 8 and 11 Hughes et al. (2012) approximated the change in overtopping discharge with time as

$$q(t) = q_N \left(1 - \frac{t}{T_O}\right)^{a+b} \tag{13}$$

where q_N [m^3/s/m] denotes the peak discharge during an individual wave overtopping event.

The peak overtopping discharge depends on the normalized run-up height to the power of 1.5. As the run-up height is linearly dependent on the breaker parameter, the mean overtopping discharge is expected to have a similar correlation with the breaker parameter. However the EurOtop manual (EurOtop, 2007) and the TAW2002 (Van der Meer, 2002) give the following relationship for the mean overtopping discharge $\overline{q}$ [m^3/s/m]

$$\frac{\overline{q}}{\sqrt{gH_s^3}} = \frac{0.067}{\tan\alpha}\gamma_b\xi_{m-1,0}\exp\left(-4.75\frac{h_c}{\xi_{m-1,0}H_s\gamma_b\gamma_f\gamma_\beta\gamma_v}\right) \tag{14}$$

with a maximum of

$$\frac{\overline{q}}{\sqrt{gH_s^3}} = 0.2\exp\left(-2.6\frac{h_c}{H_s\gamma_f\gamma_\beta}\right) \tag{15}$$

where h_c [m] denotes the crest height. These relationships both show a linear dependence on the breaker parameter $\xi_{m-1,0}$. In Section 3 a different formula is proposed for the mean overtopping discharge with a dependence on the breaker parameter to the power 1.5, which is shown to be well correlated with data from the CLASH database (Steendam et al., 2004).

2.4. Wave overtopping volume

By combining the overtopping discharge function (see Equation 13) with an expression for the overtopping volume an expression for the overtopping time

can be found. Van Gent (2002) provided a relationship for the normalized wave overtopping volume which is given by

$$\frac{V_{n\%}}{c_{Vn\%}H_s^2} = \left(\frac{R_{n\%} - z}{H_s}\right)^2 \tag{16}$$

The overtopping volume V [m^3/m] per wave follows from integrating Equation 13 with respect to time from $t = 0$ to $t = T_O$ (Hughes et al., 2012). Hofland et al. (2015) validated the hypothesis that the wave overtopping volume per wave can be described by the integral of the triangular surface area above the crest level and under the wave front at the time the wave reaches the maximum run-up height. This results in the following relationship for the overtopping volume per incident wave N, V_N [m^3/m]

$$\frac{V_N}{H_s^2} = \max\left(c_d \frac{\cos\alpha}{f_V \sin^2\alpha} \frac{R_N - h_c}{H_s^2}, 0\right) \tag{17}$$

where f_V is a shape factor for the front of the wave. For a triangular shaped wave that reduces to a zero depth $f_V = 2$. Equation 17 approximates the relationship found by Van Gent (2002).

Hughes et al. (2012) found a best fit for the volume of an individually overtopping V wave against the overtopping duration which is given by

$$V_N^{1.16} = 0.43 q_N T_O \tag{18}$$

where V [m^3/m] is the volume of an overtopping wave, the coefficient 0.43 has units [m$^{0.16}$], q_N [m^2/s] is the discharge at its maximum during an overtopping event, and T_O [s] is the overtopping time. The left hand side denotes the normalized overtopping volume. Combining Equation 18 and 16 gives

$$a + b = 2.33 V_N^{0.16} - 1 \tag{19}$$

This suggests that the shape of the overtopping discharge function (See Equation 13) becomes more concave with increase in wave volume. Hughes et al. (2012) hypothesized that more forward momentum is carried over the crest in the case of higher volumes, indicating that the power a in Equation 8 increases for larger overtopping volumes. However for small volumes ($a + b < 2$) this gives an unrealistic convex shape. Hence, a minimum value of 2 was recommended to be used for $a + b$. Hughes thereby indicated to use a maximum value of $a + b =$

4. When $b = 1$ for an assumed linear decrease in water depth with time (See Equation 11), $a = \min\left(\max(2.33V_N^{0.16} - 2, 1), 2\right)$.

The equation of Manning shows that the bed shear stress is a function of the hydraulic radius, here replaced by the water depth, and the velocity. Based on the relationships for the run-up velocity and run-up depth a relationship for the run-up bed shear stress has been derived.

2.5. Shear stress

In deriving a relationship for the bed shear stress it has been assumed that the main velocity component is parallel to the embankment surface and that the impact of other mean velocity components are negligible small in comparison. It should be noted that this may not be the case everywhere along the landside slope as due to high flow velocities the waves may separate from the landside slope. The aim behind deriving overtopping shear stress relationships is to facilitate a direct comparison between failure initiation due to overflow and wave overtopping. This comparison can be used to identify the effect of other stress components on damage initiation. For the purpose of this paper the bed shear stress is described by the following form of Manning's equation

$$\tau = \frac{\rho_w v^2 n^2}{d^{\frac{1}{3}}} \tag{20}$$

where n [s/m$^{\frac{1}{3}}$] is the Manning coefficient, v [m/s] is the main velocity component parallel to the embankment surface, and d [m] has been substituted for the hydraulic radius. To arrive at an expression for the run-up shear stress it has been assumed that the Manning equation is piece-wise valid at each instant or location. The peak shear stress can now be described as a function of the wave run-up as

$$\frac{\tau_{n\%}}{\rho_w n^2 g H_s^{2/3} (\tan\alpha)^{\frac{1}{3}} c_{\tau,n\%}} = \left(\frac{R_{n\%} - z}{H_s}\right)^{\frac{2}{3}} \tag{21}$$

where $c_{\tau,n\%} \approx \frac{c_{u,n\%}^2}{c_{d,n\%}^{1/3}}$ is the calibration parameter for the shear stress. The left hand side of Equation 21 denotes the normalized shear stress. For a stress strength analysis, or for comparing overflow with overtopping events, the parameter that is important is the excess shear stress which is defined here as the bed shear stress minus the critical shear stress. In order to arrive at a duration for which the bed shear stress exceeds the critical bed shear stress the bed shear stress has been expressed as a function of time.

Hughes et al. (2012) used Equation 18 to relate the overtopping volume and overtopping time T_O [s]. The normalized run-up parameters are related to the normalized run-up $\left(\frac{R-z}{H_s}\right)^j$, where j is a power coefficient. Replacing z with the crest height h_c [m] and expressing the values for the normalized discharge and volume in terms of normalized shear stress gives for T_O as the function of the peak shear stress

$$T_O = \frac{\tau_N^{1.23}(\tan\alpha)^{0.59}}{\rho_w^{1.23} n^{2.46} g^{1.73} 0.43 c_{\tau,n\%}^{1.23} c_{q,n\%}} \tag{22}$$

Here τ_N [N/m^2] is the peak shear stress at the intersection of the waterside slope and the crest level. According to Equation 18 the overtopping time is solely a function of the overtopping volume and the peak discharge q_N [m^3/s/m]. Once a wave overtops the volume does not change. The power that indicates the change in discharge with time is solely dependent on the volume and hence constant in space. It should be noted that this is a simplification as for an infinitely long landside slope the length of an overtopping wave will stretch out due to differences in velocity at the wave front and the tail of the wave. However, provided the assumption is reasonable this indicates that the peak discharge remains constant along the landside slope and hence that the overtopping time T_O [s] is constant. For relatively short slopes this approximation seems justifiable although further studies to the validity range of this approximation are recommended.

Although the peak discharge and volume do not change along the crest and landside slope, the depth does change. The change in depth gives a change in velocity due to local conservation of mass. From Mannings' equation follows that the shear stress τ [N/m^2] is therefore a function of the location along the crest or landside slope. How the peak shear stress changes along the crest and landside slope will be discussed in Section 2.6. First the change in shear stress with respect to time will be discussed which is described by

$$\tau(\hat{x}, t) = \tau_N(\hat{x}) \left(1 - \frac{t}{T_0}\right)^m \tag{23}$$

whereby τ, and τ_N, are functions of the location, whereby $\hat{x}$ refers to the location along the crest x or landside slope χ. Hereby $x = 0$ at the interface of the crest and waterside slope, and $\chi = 0$ at the interface of the crest and landside slope. The parameter m follows from rewriting the volume V in Equation 19 in terms of

shear stress gives

$$a+b \approx \max\left(2, 2.33 c_{V,n\%}^{1.16} \frac{\tau_{n\%}^{\frac{1}{2}}}{\rho_w^{\frac{1}{2}} n g H_s^{\frac{1}{3}} c_{\tau,n\%}^{\frac{1}{2}} (\tan\alpha)^{\frac{1}{6}}} - 1\right) \tag{24}$$

Under the assumption that the depth decreases linearly with time the power coefficient of the shear stress is approximated as

$$m = 2a - \frac{1}{3}b = \min\left(\max\left(4.66 c_{V,n\%}^{1.16} \frac{\tau_{n\%}^{\frac{1}{2}}}{\rho_w^{\frac{1}{2}} n g H_s^{\frac{1}{3}} c_{\tau,n\%}^{\frac{1}{2}} (\tan\alpha)^{\frac{1}{6}}} - 4.33, \frac{5}{3}\right), \frac{10}{3}\right) \tag{25}$$

whereby m is constant along the crest and landside slope as the volume V does not change.

For failure analysis the time domain is of importance during which the shear stress exceeds the critical shear stress. This time, denoted by t_1 [s], is given by

$$t_1(\hat{x}) = -T_O \left(\frac{\tau_c}{\tau_p(\hat{x})}\right)^{\frac{1}{m}} + T_O. \tag{26}$$

Here $\tau_p(\hat{x})$ [N/m^2] is the peak shear stress at any point on the crest or landside slope. With a change in flow velocities along the crest or landside slope the shear stress $\tau_p(x)$ also changes. Hence t_1 is also a function of location. To assess the average shear stress per overtopping wave the shear stress function needs to be integrated from $t = 0$ to $t = t_1$ which leads to

$$\begin{aligned}\int_{t=0}^{t=t_1} \tau(\hat{x},t)dt = &-\frac{T_0}{m+1}\tau_p(\hat{x})\left(\frac{\tau_c}{\tau_p(\hat{x})}\right)^{1+\frac{1}{m}} + \\ &\tau_c T_0 \left(\frac{\tau_c}{\tau_p(\hat{x})}\right)^{\frac{1}{m}} - \tau_c T_0 + \frac{T_0}{m+1}\tau_p(\hat{x})\end{aligned} \tag{27}$$

The overtopping volume and peak overtopping discharge are independent of the location along the landside slope or crest. However the peak depth, peak velocity, and peak shear stresses are a function of the location along the crest or landside slope as is discussed in the following section

2.6. Changes as a function of location

As the wave runs down the landside slope the peak bed shear stress under the wave front changes spatially due to spatial changes in peak velocity v_N [m/s] and

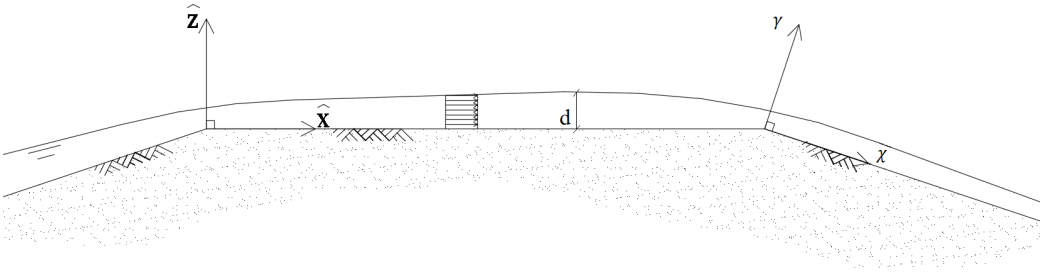

Figure 6: Run-up profile over the crest

peak depth d_N [m]. The latter follows from a depth integrated momentum balance equations. Schüttrumpf and Oumeraci (2005) provided a function that describes the change in depth along the crest and landside slope. In their derivation of this function Schüttrumpf and Oumeraci (2005) applied a steady state approximation. Inherent to this approximation the discharge is assumed constant in time and space along the landside slope. Provided mass is conserved, any change in velocity along the crest and landside slope is inversely proportional to the change in depth. Hence, effects of the local deceleration of a wave overtopping event are ignored in the derivation of Schüttrumpf and Oumeraci (2005). A second assumption made by Schüttrumpf and Oumeraci (2005) was that the pressure gradient term in x-direction is 0 at the free surface. In doing so, the pressure gradient term was removed from the momentum balance equation prior to integrating the equation over the height. Hence in the analysis of Schüttrumpf and Oumeraci (2005) the water level gradient was removed from the momentum balance equation in determining the analytical solution for the spatial change in depth. Below an attempt was made to improve on the relationship given by Schüttrumpf and Oumeraci (2005) by accounting for the local change in discharge with time, and the depth integrated pressure gradients. The starting point of the analysis are the generic one-dimensional Shallow Water Equations for a steady state flow, which for a unit width, slip conditions at the sides, an hydraulic radius equal to the depth, and a landside slope with angle β, are given by

$$\frac{\partial q}{\partial t} + \frac{\partial}{\partial d}\left(\frac{q^2}{d} + g\cos\beta\frac{1}{2}d^2\right)\frac{\partial d}{\partial \hat{x}} - gd\sin\beta + c_f\frac{q^2}{d^2} - Sq = 0, \qquad (28)$$

where d [m] is the depth, q [m^3/s/m] the breadth averaged discharge component parallel to the bed, h [m] the water level, g [m/s^2] the gravitational constant, c_f is a

friction factor, and S is a source term given by $S = \frac{1}{\rho_w}\frac{d\rho_w}{dt}$ [s^{-1}]. $\hat{x}$ is the direction perpendicular to the embankment whereby $\hat{x} = x$ for a flow over the crest and $\hat{x} = \chi$ for a flow down the landside slope (see Figure 6). For the analysis no mass is assumed to be lost during the flow over the crest. For simplicity, the shear stress has been determined by

$$\tau = c_f \frac{q^2}{d^2} \tag{29}$$

Manning's equation can be found by substituting $c_f \approx \frac{gn^2}{d^{1/3}}$. The magnitude of the discharge component q is assumed to match the breadth averaged discharge. Taking the water depth perpendicular to the embankment surface leads to the following differential equation for the water depth on the crest ($\beta = 0$)

$$\frac{\partial d}{\partial x} = \frac{-c_f q^2 - d^2\left(\frac{\partial q}{\partial t} - Sq\right)}{-q^2 + gd^3} \tag{30}$$

Under the assumption that the local change in discharge with time remains constant it is possible to define an artificial depth d_a [m] as

$$d_a^2 = -\frac{c_f q^2}{q_t - Sq} \tag{31}$$

whereby $q_t = \frac{\partial q}{\partial t}$ [m^3/s^2/m]. Also a critical depth d_c [m] is defined as

$$d_c^3 = \frac{q^2}{g}. \tag{32}$$

For small deviations of the depth from the artificial depth d_a [m] the depths could be approximated by $d = d_a + \Delta d$, which gives for Equation 30

$$\frac{\partial \Delta d}{\partial x} = \frac{(2d_a \Delta d(q_t - Sq) + O\left(\Delta d^2\right))}{\left(g\tilde{d_a^3} - g\tilde{d_c^3} + 3gd_a^2\Delta d + O(\Delta\tilde{d})^2\right)} \tag{33}$$

For small deviations from the artificial depth d_a, the terms of $O\Delta d^2$ can be ignored, leading to.

$$\left(g\frac{d_a^3 - d_c^3}{\Delta d} + 3gd_a^2\right)\mathrm{d}\Delta d = 2d_a(q_t - Sq)\mathrm{d}x \tag{34}$$

or

$$\exp\left(\frac{3d_a\Delta d}{d_a^3 - d_c^3}\right)\Delta d = \exp\left(\frac{2d_a(q_t - Sq)\Delta x}{g\left(d_a^3 - d_c^3\right)}\right) \tag{35}$$

Working this out and using the Taylor expansion of $\Delta d e^{a\Delta d}$ around 0, and applying the boundary condition that $d = d_a + d_0$ at $x = x_0$ one gets the following approximation with an error of the order Δd^2

$$d(x) = d_a + d_0 \text{exp}\left(\frac{2d_a(q_t - Sq)(x - x_0)}{g\left(d_a^3 - d_c^3\right)}\right) \tag{36}$$

where x_0 is the location where the water depth $d(x)$ [m] matches the run-up depth on top of the waterside slope. This derivation differs from that of Van Gent (2002) and Schüttrumpf and Oumeraci (2005) in the sense that it accounts for the effects of the local deceleration of an overtopping wave. The effect of this is that the water depth increases along the crest unless the source term multiplied by the discharge exceeds the acceleration term ($Sq > q_t$). Both for $S = 0$ and $S < 0$ the flow velocities decrease which corresponds with the description given in the EurOtop manual. (EurOtop, 2007).

For the flow along the landside slope ($\beta > 0$), a χ, γ coordinate system has been defined such that χ is parallel along the landside slope and γ is normal to χ as given in Figure 6. With a water depth $\tilde{d}$ measured perpendicular to the landside slope, a flow velocity component $\tilde{v}$ parallel to the slope, and $\tilde{q} = \tilde{d}\tilde{v}$[m^3/s/m], the following differential equation is found from the 1D momentum balance equation

$$\frac{\partial \tilde{d}}{\partial \chi} = \frac{-c_f \tilde{q}^2 + g\tilde{d}^3 \text{sin}\beta - \tilde{d}^2 \tilde{q}_t}{\left(\text{cos}\beta g\tilde{d}^3 - \tilde{q}^2\right)} \tag{37}$$

It has thereby been assumed that the other velocity components are negligibly small compared to the main velocity component. For the derivation of the analytical solution an artificial depth, $\tilde{d}_a$ [m] has been derived given by

$$g\tilde{d}_a^3 \text{sin}\beta - \tilde{q}_t \tilde{d}_a^2 = c_f \tilde{q}^2 \tag{38}$$

For a steady state flow $q_t = 0$ and d_a becomes equal to the normal depth. The critical depth $\tilde{d}_c$ is defined as

$$\tilde{d}_c^3 = \frac{\tilde{q}^2}{g\text{cos}\beta} \tag{39}$$

Substitution of $\tilde{d} = \tilde{d}_a + \Delta\tilde{d}$ gives for Equation 37

$$\frac{\partial \Delta\tilde{d}}{\partial \chi} = \frac{g\text{sin}\beta\left(3\tilde{d}_a^2 \Delta\tilde{d} + O(\Delta d^2)\right) - \tilde{q}_t\left(2\tilde{d}_a \Delta\tilde{d} + O(\Delta\tilde{d}^2)\right)}{-g\text{cos}\beta\tilde{d}_c^3 + g\text{cos}\beta\left(\tilde{d}_a^3 + 3\tilde{d}_a^2\Delta\tilde{d} + O(\Delta\tilde{d}^2)\right)} \tag{40}$$

For small deviations from the artificial depth $\tilde{d}_a$ [m], the term $O\Delta\tilde{d}^2$ can be ignored, leading to

$$g\text{cos}\beta\left[\left(\tilde{d}_a^3-\tilde{d}_c^3\right)\ln\left(\Delta\tilde{d}\right)+3\tilde{d}_a^2\Delta\tilde{d}\right]=\left(3g\text{sin}\beta\tilde{d}_a^2-q_t\tilde{d}_a^2\right)\chi \tag{41}$$

Working this out and using the Taylor expansion of $\Delta\tilde{d}e^{a\Delta\tilde{d}}$around 0, substituting that $\tilde{d}=\tilde{d}_a+\Delta\tilde{d}$, and applying the boundary condition that $\tilde{d}=\tilde{d}_a+\tilde{d}_0$ at $\chi=\chi_0$ the following approximation is found for the depth as a function of χ with an error of the order $\Delta\tilde{d}^2$

$$\tilde{d}(\chi)=\tilde{d}_a+\tilde{d}_0\text{exp}\left(\frac{\left(3g\text{sin}\beta\tilde{d}_a^2-q_t\tilde{d}_a^2\right)(\chi-\chi_0)}{\tilde{d}_a^3-\tilde{d}_c^3}\right) \tag{42}$$

Here χ_0 is the location where the water depth $d(\chi)$ matches the depth $\tilde{d}_a+\tilde{d}_0$. The EurOtop manual gives for the terminal velocity for an overtopping wave along the landside slope

$$\tilde{v}_b=\sqrt{\frac{2g\tilde{d}_b\text{sin}\beta}{f}} \tag{43}$$

where $\tilde{v}_b$ is the terminal velocity, $\tilde{d}$ is the corresponding water depth measured perpendicular to the slope, and f is a friction parameter with an approximate value of 0.22. multiplying the left and right side by the depth $\tilde{d}_b$ gives after some manipulation

$$\tilde{d}_b^3=\frac{q^2f}{2g\text{sin}\beta} \tag{44}$$

Comparing Equation 44 with Equation 38 shows that for $d_a=d_b$, the effects of deceleration $(q_t<0)$ result in higher friction values. Equation 43 inherently assumes the effects of deceleration to be negligible whereas this leads to a significant underestimation of the shear stresses on the embankment surface. For a landside slope gradient of $1/3$ and a peak discharge of 1.3m^3/s a manning parameter of $0.025\text{s/m}^{1/3}$ gives the same terminal velocity and depth as a manning parameter of 0.054 s/m$^{1/3}$ when flow deceleration is accounted for. As the shear stress is quadratically dependent on the Manning coefficient, this gives a 4.6 times higher shear stress prediction when accounting for the deceleration effects and when these are ignored.

Assuming that the peak discharge along the crest and the landside slope remains constant the change in velocity is inversely proportional to the change in

depth. The shear stress at any point along the crest and landside slope is now found by multiplying the shear stress by a depth dependent factor. According to Manning's Equation the shear stress is proportional to

$$\tau :: \frac{u^2}{\tilde{d}^{\frac{1}{3}}} \tag{45}$$

and hence as the depth decreases along the landside slope the maximum value for the shear stress increases according to

$$\tau_N(\hat{x}) = \left(\frac{\tilde{d}_{N,0}}{\tilde{d}(\hat{x})} \right)^{\frac{7}{3}} \tau_{N,0} \tag{46}$$

where $\tau_{N,0}$ [N/m^2] and $\tilde{d}_{N,0}$ [m] are respectively the peak shear stress and peak depth at $\hat{x} = 0$.

With relationships for the velocity, depth, discharge, volume, and shear stress in place, distributions have been developed for each of these parameters assuming Rayleigh distributed incoming waves. The following paragraph describes the development of these distributions.

3. Distribution of wave overtopping parameters

The different wave parameters given in Section 2, have been described by the generic equation

$$N = \left(\frac{R_{n\%} - h_c}{H_s} \right)^j \tag{47}$$

where N is a normalized wave overtopping parameter. For $j = \frac{1}{2}$, N describes the normalized run-up velocity at crest level, for $j = \frac{2}{3}$ the normalized run-up bed shear stress at crest level, for $j = 1$ the normalized run-up depth at crest level, for $j = 1.5$ the normalized run-up discharge at crest level, and for $j = 2$ the normalized unit overtopping volume (See Equations 5, 9, 12, 16, and 21). These variables are respectively denoted by U_p, $\mathcal{T}_p$, D_p, Q_p, and V. Besides the significant wave height H_s, the run-up height is also a function of the parameter

$$\epsilon = \min \left\{ \xi_{m-1,0} \gamma_b \gamma_\beta \gamma_f, \frac{\gamma_f \gamma_\beta}{1.65} \left(4.0 - \frac{1.5}{\sqrt{\xi_{m-1,0}}} \right) \right\} \tag{48}$$

Hence, any distribution describing the wave overtopping parameters is a function of Equation 48. The cumulative distribution function of the Rayleigh distribution is given by

$$F(x,\sigma) = 1 - \exp\left(-\frac{x^2}{2\sigma^2}\right) \text{ for } x > 0 \tag{49}$$

The run-up is Rayleigh distributed and follows from $R = H_s \epsilon x$, or $x = \frac{R}{H_s \epsilon}$. Substituting this expression in the Rayleigh distribution gives

$$F(R,\sigma) = 1 - \exp\left(-\frac{R^2}{2\sigma^2 \epsilon^2 H_s^2}\right) \text{ for } R > 0 \tag{50}$$

whereby $\sigma = \sqrt{\frac{0.93^2}{2}} = 0.658$, which follows from Equation 3. Equation 50 is the general cumulative distribution function for up-running waves.

The overtopping volume can be approximated by the amount of up-running water that exceeds the crest level. The length over which water runs up is given by $\frac{R-h_c}{\sin\alpha}$. Assuming that the depth decreases linearly with the run-up height the total volume V follows from

$$\frac{V}{H_s^2} = \max\left(\frac{c_d}{f_V}\frac{\cos\alpha}{\sin^2\alpha}\frac{(R-h_c)^2}{H_s^2}, 0\right) \tag{51}$$

from which follows that

$$R = \left(\frac{f_V \sin^2\alpha}{\cos\alpha c_d} V\right)^{\frac{1}{2}} + h_c \text{ for } R > h_c \tag{52}$$

Substituting this expression for R in Equation 51 gives the survivor function for the overtopping volume V

$$F(V,\sigma) = P(V > V) = \exp\left[-\frac{\left(\frac{f_V \sin^2\alpha}{\cos\alpha c_d}\right) V + 2h_c \left(\frac{f_V \sin^2\alpha}{\cos\alpha c_d} V\right)^{\frac{1}{2}} + h_c^2}{2\sigma^2 H_s^2 \epsilon^2}\right] \tag{53}$$

Equation 53 describes the probability P of individual waves overtopping the crest level h_c and exceeding the overtopping volume V. Because not every wave reaches the crest level the integral of Equation 53 does not integrate to 1. Hence to arrive at the cumulative distribution function for the wave overtopping volume for those

waves that do overtop it is necessary to normalize Equation 53 by the probability that the run-up level exceeds the crest level. This is is given by

$$F(R > h_c) = \exp\left(-\frac{h_c^2}{2\sigma^2 H_s^2 \epsilon^2}\right) \tag{54}$$

Dividing Equation 53 by Equation 54 gives the cumulative distribution function for overtopping waves which is equal to

$$F(V,\sigma) = 1 - \exp\left[-\frac{\left(\frac{f_V \sin^2\alpha}{\cos\alpha c_d}\right) V + 2h_c \left(\frac{f_V \sin^2\alpha}{\cos\alpha c_d} V\right)^{\frac{1}{2}}}{2\sigma^2 H_s^2 \epsilon^2}\right] \tag{55}$$

The distribution shape given by Equation 55 was compared against the overtopping volume distributions from the EurOtop manual and the improvements made by Zanuttigh and Lamberti (2007). Both assume that the wave overtopping Volume is Weibull distributed whereby the scale factor follows from $a = 0.84 T_m \frac{q}{P_{\text{ot}}}$. Here T_m is the mean wave period, q is the mean wave overtopping discharge, and P_{ot} is the probability of overtopping. The mean overtopping discharge parameter used in these distributions was obtained from Equations 14 and 15. In the EurOtop manual the shape factor is set to 0.75, whereas Zanuttigh and Lamberti (2007) suggested a shape factor b given by $b = 0.73 + 55\left(\frac{q}{g H_s T_{m-1,0}}\right)^{0.8}$. Hence both these methods are dependent on the mean wave overtopping discharge q. The standard deviations of the exponents in respectively Equation 14 and 15 are 0.5 and 0.35 (Zanuttigh and Lamberti, 2007). The coefficient of variance corresponding with predictions of the mean overtopping discharge (see Equations 14 and 15) was determined from the CLASH database for those cases with negligible friction losses, normally incoming waves, and no berm. This results in a coefficient of variance of 2. Unlike the current state of the art relationships for the overtopping volume, Equation 55 is independent on the mean overtopping discharge and hence independent on the uncertainties associated with the mean overtopping discharge.

The overtopping volume predictions have been plotted against the probability of exceedance for normally incoming Rayleigh distributed waves with a significant wave height of 0.95m, a friction parameter of 1, and a breaker parameter of 3.1 . Figures 7 and 8 respectively show the comparison between the results from Equation 55, the method from the EurOtop Manual (EurOtop, 2007), and the improvements on the EurOtop method by Zanuttigh and Lamberti (2007) for respectively a crest level equal to the 2% run-up level, and 50% run-up level. As shown

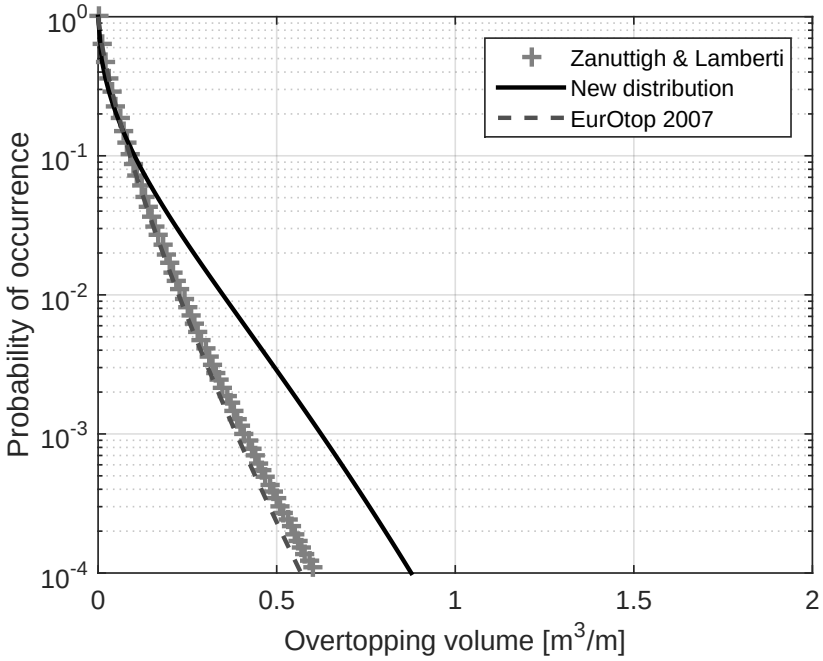

Figure 7: Comparison of the overtopping volumes as a function of probability of overtopping for a design crest level with a 2% overtopping probability

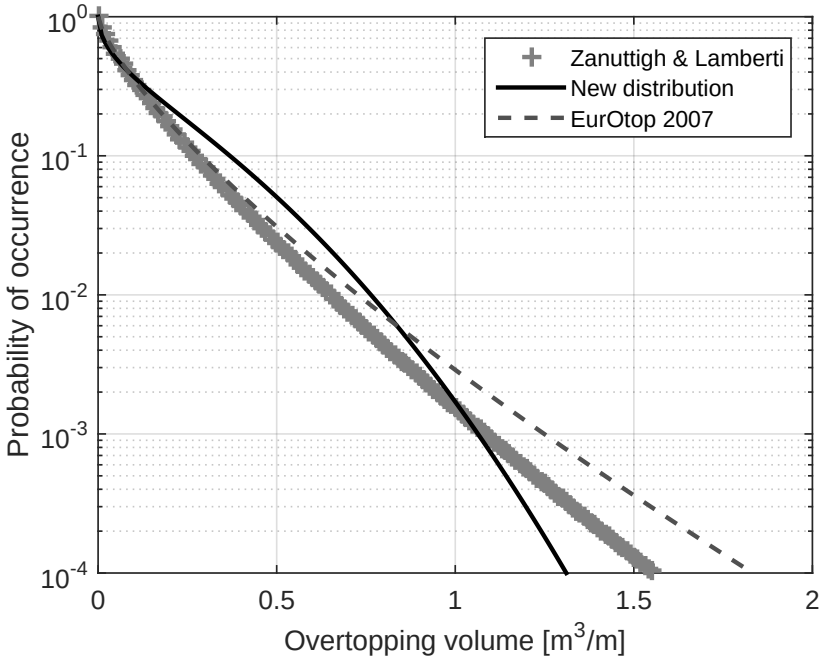

Figure 8: Comparison of the overtopping volumes as a function of probability of overtopping for a design crest level with a 50% overtopping probability

in the Figure 7, the newly developed method gives a higher prediction for the overtopping volume for low probability events. Differences in the general shape of the distribution follow from the differences between shape of the distribution given by Equation 55 and the Weibull distribution. Figure 8 shows a similar trend at first but as the probability decreases further the predictions from the proposed method become lower than the volume predictions following from the method by Zanuttigh and Lamberti (2007). The assumptions underlying these plots are that the depth decreases linearly with the run-up height according to Equation 10, and that the overtopping volume is given by the fraction of a prism shaped run-up volume that exceeds the crest level. Lower predictions for the overtopping volume would be found when it is assumed that part of the volume, for which the wave run-up exceeds the crest level, flows back down the waterside slope. Hence Equation 55 gives an upper limit for the overtopping volume for waves whose run-up depth decreases linearly with the run-up height. Hence regions for which Equation 55 under-predicts the wave overtopping volumes, indicate that the assumption of a linear reduction in run-up depth may be invalid, or that the coefficient $c_{d,n\%}$ is different for different probability events. However as the ratio in predictions given in Figures 7 and 8 is smaller than the coefficient of variance of 2 corresponding with the shape factors of the Weibull distributions it would be challenging to determine the source of errors in the predictions given by Equation 55.

Based on the analysis above a more general form of Equation 53 could be created for overtopping parameters like the overtopping depth, velocity, discharge and shear stress. Starting from Equation 50, the generic substitution equation is then given by

$$R = c_X X^{\frac{1}{j}} + h_c \tag{56}$$

Substituting this expression in Equation 50 and correcting the equation for those waves that do overtop gives

$$F(X,\sigma) = 1 - \exp\left(\frac{h_c^2}{2\sigma^2 H_s^2 \epsilon^2}\right) \exp\left\{-\frac{\left[(c_X X)^{\frac{1}{j}} + h_c\right]^2}{2\sigma^2 H_s^2 \epsilon^2}\right\} \tag{57}$$

The values for c_X depend on the parameter of interest and are given by Table 2.

The dependance between the overtopping velocity and crest height $j = 0.5$ follows directly from the energy balance. However the linear dependance between the overtopping depth and crest height $(j = 1)$ is purely determined empirically. The overtopping discharge follows from the overtopping depth multiplied by the

Parameter	symbol	c_X
Overtopping velocity	U_p	$\frac{1}{c_u\sqrt{g}} \approx \frac{1}{\sqrt{2g}}$
Overtopping shear stress	$\mathcal{T}_p$	$\frac{1}{\rho_w n^2 g \tan\alpha c_\tau}$
Overtopping depth	D_p	$\frac{\tan\alpha}{c_d} \approx \frac{\tan\alpha}{0.055}$
Overtopping discharge	Q_p	$\frac{\tan\alpha}{c_d\sqrt{g}} \approx \frac{\tan\alpha}{0.055\sqrt{g}}$
Overtopping Volume	V	$\frac{f_V \sin^2\alpha}{\cos\alpha c_d} \approx \frac{2\sin^2\alpha}{0.055\cos\alpha}$

Table 2: Parameters for the Weibull distribution for the normalized depths of overtopping waves $\left(\frac{R-h_c}{H_s}\right)$ for a 10% crest level

overtopping velocity, and hence depends on the accuracy with which the run-up depth is described. Because the new distributions have been derived by expressing the overtopping parameters in terms of the Rayleigh distributed run-up, the overtopping parameters can also be expressed in terms of each other. Comparing the relationship for the peak overtopping volume with the peak overtopping discharge gives

$$\left(\frac{\sin^2\alpha}{\cos\alpha c_d} V\right)^{\frac{1}{2}} = \left(\frac{c_d\sqrt{g}}{\tan\alpha} q_p\right)^{\frac{2}{3}} \tag{58}$$

Equation 58 shows that the peak overtopping discharge is proportional to overtopping volume according to

$$q :: \sqrt{g} V^{\frac{3}{4}} \tag{59}$$

which was also found empirically by Hughes et al. (2012). Assuming that the peak overtopping discharge and mean overtopping discharge are fully correlated the dependencies of the overtopping parameters on the run-up height have been evaluated using the mean overtopping discharge predictions given by the CLASH database. The current mean overtopping relationships given by Equation 14 and 15 show a correlation with the data from the CLASH database of 0.88 for those cases whereby the berm widths are 0, the angle of wave attack is normal to the levee, and the friction losses are negligible. The peak overtopping discharge distribution for those waves that overtop is given by

$$P = \exp\left\{-\frac{\left[(c_q q)^{\frac{2}{j}} + 2h_c (c_q q)^{\frac{1}{j}}\right]}{2\sigma^2 H_s^2 \epsilon^2}\right\} \tag{60}$$

For $P = 0.8$ the peak overtopping discharges were found to match empirically the averaged overtopping discharge during overtopping events $\overline{q_{ot}}$ [m^3/s/m]. The

value of $P = 0.8$ indicates that 80% of the overtopping discharges exceed the predicted value. The CLASH database (Steendam et al., 2004) contains values on the mean overtopping discharge defined as the total overtopping volume divided by the total experimental time. Hence normalizing $\overline{q_{ot}}$ by the probability of an overtopping event results in the mean overtopping discharge $\overline{q}$ [m^3/s/m] given by

$$\overline{q} = \overline{q_{ot}} \exp\left(-\frac{h_c^2}{2\sigma^2 H_s^2 \epsilon^2}\right) \tag{61}$$

The relationship between the prediction from Equation 61 and the CLASH database has been depicted in Figure 9 together with the fit between the data and the prediction obtained from Equations 14 and 15. Equation 61 gives a correlation with the data of 0.86 whereas Equations 14 and 15 give a correlation with the data of 0.88 indicating that a similar good match can be obtained using this approach.

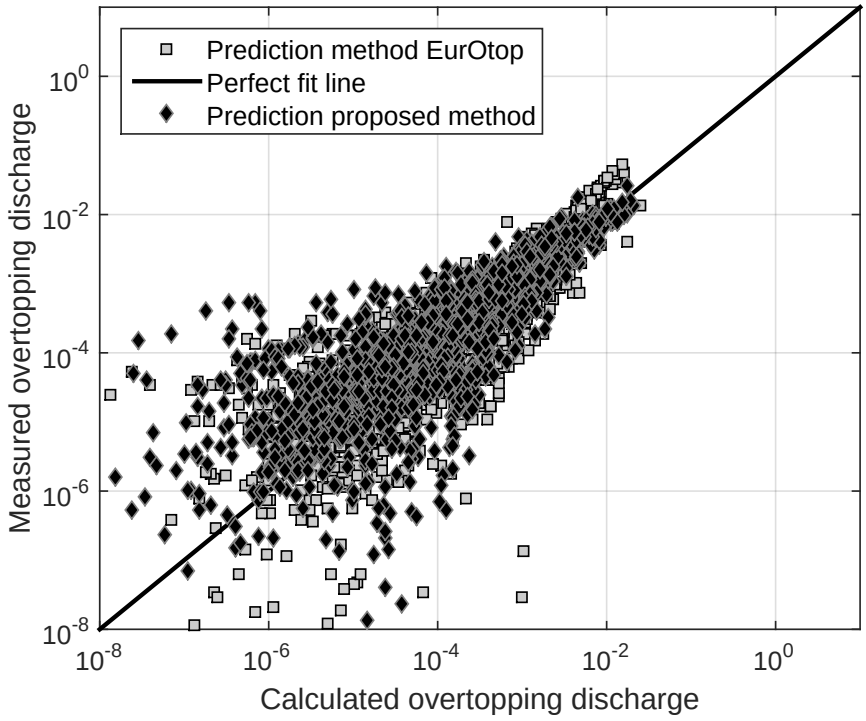

Figure 9: Comparison of the calculated mean overtopping discharges with the measured mean overtopping discharges from the CLASH database

4. Discussion

Over the past years much experimental research has been performed on wave run-up and overtopping. The test parameters and mean overtopping discharge measured during these tests have been collected in the CLASH database. The coefficient of variance of the current state of the art prediction methods for the mean overtopping discharge is 2, indicating a high level of uncertainty. The scale parameters of the Weibull shaped overtopping volume distributions (EurOtop, 2007; Zanuttigh and Lamberti, 2007) are linearly dependent on the mean overtopping discharge predictions transferring this high level of uncertainty to the wave overtopping volume predictions.

This paper provides new distributions for a variety of overtopping parameters by expressing the overtopping parameters in terms of the Rayleigh distributed run-up height and thereby making them independent on the mean overtopping discharge. Coefficients for use in the distributions (See Table 2) have been derived by analyzing theory and data (Hofland et al., 2015). The theoretical analysis shows that for smooth slopes the effects of friction are small when determining wave run-up velocities. The data analysis shows that the water level gradient at maximum run-up levels is approximately constant over a large range but appears to decrease near the wave front. Based on this, empirical coefficients are given for the distributions of the overtopping discharge, overtopping volume, and overtopping shear stress. Because each of these overtopping parameters are described in terms of the normalized difference between run-up levels and crest level, the parameters are expressible in terms of each other. The proportionality between the wave overtopping volumes and peak overtopping discharge found this way corresponds with the proportionality found by Hughes et al. (2012).

The ratio between predictions following from the developed distribution for wave overtopping volumes (Equation 55) and the Weibull distribution (EurOtop, 2007) is small compared to the coefficient of variance associated with the mean overtopping discharge parameter on which the scale parameters of the Weibull distribution (EurOtop, 2007) are linearly dependent. The match in proportionality with the findings of Hughes et al. (2012) combined with the relative small difference in predictive capabilities with the current state of the art Weibull distribution indicates the viability of the new method. The proposed distributions are thereby likely to have a coefficient of variance which is smaller than the ones dependent on the mean overtopping discharge. A second benefit of the new distributions is that each wave overtopping parameter is easily expressed in terms of the others, an example of which has been given in Equation 58. The shear stress distribution

could directly be used for comparing the shear stresses at crest level during wave overtopping events with the shear stresses at crest level during overflow events.

A process based analysis has been performed to derive equations that describe the change in overtopping parameters as a function of the location along the crest or landside slope. When developing these equations it was noted that the local acceleration term has a significant effects on the equilibrium depth prediction, or shear stress prediction. Accounting for the deceleration in the momentum balance equations results in a significantly higher bed shear stress prediction. Before using these equations it should furthermore be noted that the flow is assumed as one-dimensional. When waves overtop the embankment the flow could separate from the landside slope near the landside end of the crest. Until the wave has reattached with the embankment surface the equations describing the change in depth profile are invalid as the processes conflict with the underlying assumption of having a hydrostatic pressure distribution.

5. Conclusions

The analysis presented in this paper has led to several new distributions for describing respectively the overtopping depth, velocity, discharge, shear stress, and volume at crest level. These distributions have been derived by expressing overtopping parameters in terms of wave run-up parameters. Coefficients for use in the distributions have also been given. The new distribution are independent on the mean overtopping discharge and hence the coefficient of variance of the mean wave overtopping discharge relationships are not transferred into the shape or scale parameters of the distribution. The distributions proposed in this paper thereby allows for easy transformation of one overtopping parameter in another. Equations for the spatial change in parameters have also been derived. Together these provide a good initial means of comparing the stresses on embankments during overflow and overtopping events, and for performing a stress/strength analysis. Further study to the validity range of these equations is however recommended.

6. Acknowledgements

This research was performed as part of the STW project SAFElevee. The author would like to thank STW for making this research possible. Furthermore the author would like to thank Paul van Steeg for providing data on the run-up heights, Oswaldo Morales Napoles for his asistence with the statistical approach, and Bas Hofland for making data available for analyzing the gradients in run-up depth.

7. Bibliography

Battjes, J., 1974. Computation of set-up, longshore currents, run-up and overtopping due to wind-generated waves. Ph.D. thesis, Delft University of Technology.

Dean, R., Rosati, J., Walton, T., Edge, B., Jan 2010. Erosional equivalences of levees: Steady and intermittent wave overtopping. Ocean Engineering 37, 104–113.

D'Eliso, C., 2007. Breaching of sea dikes initiated by wave overtopping: A tiered and modular modelling approach. Ph.D. thesis, University of Florence.

Environment Agency, 2009. Flooding in England: A national assessment of flood risk. In: Flooding and coastal change. No. LIT4036. Environment Agency, pp. 1–36.

EurOtop, 2007. Wave Overtopping of Sea Defences and Related Structures: Assessment Manual.
URL `www.overtopping-manual.com`

Gouldby, P. B., Sayers, B. P., Panzeri, M., Lanyon, J., 2010. Development and application of efficient methods for the forward propagation of epistemic uncertainty and sensitivity analysis within complex broad-scale flood risk system models. Canadian Journal of Civil Engineering, 955–967.

Hall, W. J., Meadowcroft, C. I., Sayers, P., Bramley, M., 2003. Integrated flood risk management in england and wales. Natural Hazards Review, 126–135.

Hofland, B., Diamantidou, E., Van Steeg, P., Meys, P., 2015. Wave runup and wave overtopping measurements using a laser scanner. Coastal Engineering 106, 20–29.

Hughes, S., May 2011. Adaptation of the levee erosional equivalence method for the hurricane storm damage risk reduction system (hsdrrs). Tech. rep., US Army Core of Engineers, Engineer Research and Development Center.

Hughes, S. A., Thornton, C., Van der Meer, J., Scholl, B., 2012. Improvements in describing wave overtopping processes. In: Lynett, P., Smith, J. (Eds.), Coastal Engineering 2012. No. 33.

Hunt, A. I., 1959. Design of seawalls and breakwaters. Journal of Waterways and Harbours Division 85, 123–152.

Kuijken, W., 2015. Deltaprogramma 2015, werk aan de delta.
URL www.deltacommissaris.nl/deltaprogramma/inhoud/publicaties

Macchione, F., 2008. Model for predicting floods due to earthen dam breaching. Journal of Hydraulic Engineering-ASCE, 1688–1696.

Schüttrumpf, H., Oumeraci, H., 2005. Layer thickness and velocities of wave overtopping flow at seadikes. Coastal Engineering 52, 473–495.

Singh, P. V., Scarlatos, D. P., Collins, G. J., Jourdan, R. M., 1988. Breach erosion of earthfill dams (beed) model. Natural Hazards 1, 161–180.

Steendam, G. J., Van der Meer, J. W., Verhaeghe, H., Besley, P., Franco, L., Van Gent, M. R. A., 2004. The international database on wave overtopping. In: Hansen, H., Deigaard, R., Drønen, N. (Eds.), Coastal Engineering 2004. No. 29.

Van der Meer, W. J., 2002. Technisch rapport golfoploop en golfoverslag bij dijken, (dutch). Tech. rep.

Van der Meer, W. J., Bernardini, P., Snijders, W., Regeling, E., 2006. The wave overtopping simulator. In: Smith, J. (Ed.), Coastal Engineering 2006. No. 30. World Scientific, pp. 4654–4666.

Van der Meer, W. J., Steendam, J. G., de Raat, G., Bernardini, P., 2008. Further developments on the wave overtopping simulator. In: Smith, J. (Ed.), Coastal Engineering 2008. World Scientific.

Van Gent, M., 2002. Low-exceedance wave overtopping events, measurements of velocities and the thickness of water-layers on the crest and inner slope of dikes. Tech. rep.

Van Steeg, P., 2015. Personal correspondencee with Paul van Steeg (Deltares).

Wu, W., 2013. Simplified physically based model of earthen embankment breaching. Journal of Hydraulic Engineering-ASCE, 837–851.

Zanuttigh, B., Lamberti, A., 2007. Instability and surge development in debris flows. Reviews of Geophysics 45.

Zhu, Y., 2006. Breach growth in clay-dikes. Ph.D. thesis, Delft University of Technology.